Additive Manufacturing 35 (2020) 101309

Contents lists available at ScienceDirect

Additive Manufacturing

journal homepage: www.elsevier.com/locate/addma

Research paper

An ultrasonic metallic Fabry–Pérot metamaterial for use in water

Meisam Askari[a], David A. Hutchins[b,*], Richard L. Watson[b], Lorenzo Astolfi[b], Luzhen Nie[c], Steven Freear[c], Peter J. Thomas[b], Stefano Laureti[d,e], Marco Ricci[e], Matt Clark[f], Adam T. Clare[a]

[a] Department of Mechanical, Material and Manufacturing Engineering, University of Nottingham, University Park, Nottingham, NG7 2RD, UK
[b] School of Engineering, University of Warwick, Coventry, CV4 7AL, UK
[c] School of Electronic and Electrical Engineering, University of Leeds, Leeds, LS2 9JT, UK
[d] Department of Engineering, University of Perugia, Strada Di Pentima n.4-05100, Terni, Italy
[e] Department of Informatics, Modelling, Electronics and System Engineering, University of Calabria, 87036 Rende, Italy
[f] Optics and Photonics, Faculty of Engineering, University of Nottingham, University Park, Nottingham, NG7 2RD, UK

ARTICLE INFO

Keywords:
Acoustic metamaterials
Additive manufacturing
Selective laser melting
Fabry–Pérot resonance

ABSTRACT

Fabry-Pérot ultrasonic metamaterials have been additively manufactured using laser powder bed fusion to contain subwavelength holes with a high aspect-ratio of width to depth. Such metamaterials require the acoustic impedance mismatch between the structure and the immersion medium to be large. It is shown for the first time that metallic structures fulfil this criterion for applications in water over the 200–800 kHz frequency range. It is also demonstrated that laser powder bed fusion is a flexible fabrication method for the ceration of structures with different thicknesses, hole geometry and tapered openings, allowing the acoustic properties to be modified. It was confirmed via both finite element simulation and practical measurements that these structures supported Fabry-Pérot resonances, needed for metamaterial operation, at ultrasonic frequencies in water. It was also demonstrated the the additively-manufactured structures detected the presence of a sub-wavelength slit aperture in water.

1. Introduction

Acoustic metamaterials are those that have properties that arise from their inner structure and which are not ordinarily observed. For example, extraordinary effects can occur when acoustic signals are transmitted through multiple holes in a solid plate. This can occur when the diameter of the holes is less than the acoustic wavelength and when the hole exhibits an acoustic resonance [1]. Unlike the optical equivalent, there is no lower cut-off frequency for sound waves, and information can be transmitted through the sub-wavelength holes from one side of a perforated plate to the other [2]. Provided the hole is deep enough, propagation of acoustic waves within subwavelength-sized apertures can lead to the formation of Fabry-Pérot (FP) transmission resonances within each hole. FP resonance is produced by the constructive and destructive interference of waves confined in the holes that can produce multiple transmission peaks [3]. If an array of such holes are placed side-by-side, an acoustic metamaterial is created with some novel properties such as subwavelength acoustic imaging [3]. This is made possible by coupling the evanescent waves which exist within the fluid close to the sample and the FP resonance within each hole.

Zhu et al. [4] have demonstrated that, at audible acoustic frequencies in air, features can be funnelled through a set of subwavelength apertures to produce acoustic images. This happens at frequencies at which the FP resonances within each hole occur, provided the holes are sufficiently close together across the metamaterial [5]. Such structures are of interest for ultrasonic imaging at subwavelength resolutions, holding promise for improved medical imaging and non-destructive evaluation [4,6,7]. However, this requires operation at higher frequencies and in water. To date, most research in this area has been based on either numerical simulations of these structures [6,8] or experimental measurements in air on samples fabricated using conventional machining. Examples include assembling tubes in an array and bonding them using glue for audible range applications in air [4], or drilling holes into a metallic plate [3,8,9]. The expected FP resonances were observed [8,10]. A number of publications have studied the effects of dimension, shape, symmetry and filling fraction of the holes on the acoustic response of such perforated plate structures [2,11–13]. Laureti et al. [9] suggested that by decreasing the hole dimension, the position of the FP peaks shift to higher frequencies and the peak amplitude increases.The effect of hole filling fraction (the fraction of the material containing holes compared to solid substrate) was also

* Corresponding author.
E-mail address: d.a.hutchins@warwick.ac.uk (D.A. Hutchins).

https://doi.org/10.1016/j.addma.2020.101309
Received 16 October 2019; Received in revised form 27 March 2020; Accepted 30 April 2020
Available online 15 May 2020

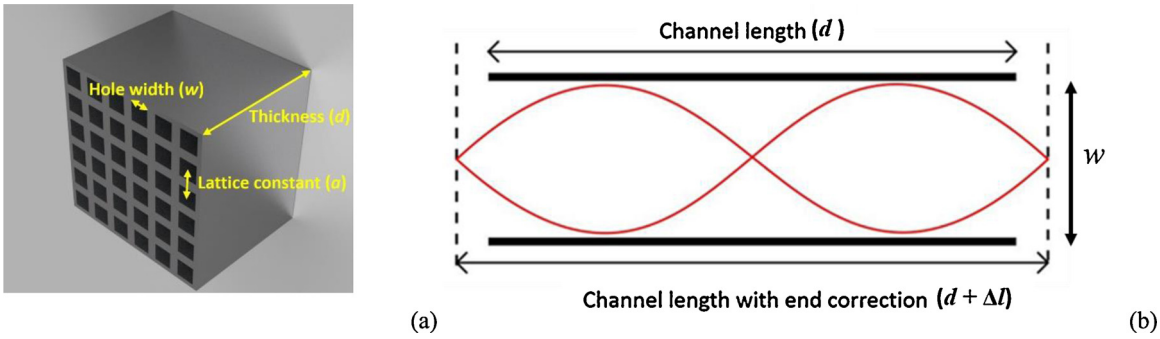

Fig. 1. (a) Schematic diagram of an FP metamaterial containing square holes, and (b) the effect of end correction Δl (for the second natural frequency (f_2) of an open channel).

studied and it was confirmed that by increasing the filling fraction the resonance peak shifts to higher frequencies and the transmission peaks become narrower [14]. Therefore, the resolution of the resultant metamaterial would be improved by decreasing the hole diameter and increasing the filling fraction [15]. The signal transmitted through a periodically perforated structure is affected not only by FP resonances within each hole, but also any acoustic signal that travels either along the surfaces of the solid material or within it. The interaction between these phenomena produces a complex transmission curve with maxima and minima at different frequencies [14].

A schematic diagram of a typical FP acoustic metamaterial is shown in Fig. 1(a). It is important that both the hole width (w) and the distance between hole centres are smaller than the acoustic wavelength (λ) for metamaterial behaviour to be observed [8], as this is needed for evanescent wave coupling between each hole. When the acoustic frequencies are low, then conventional machining is sufficient for sample preparation (for example, at 10 kHz the wavelength λ_{air} in air is ~33 mm for an acoustic velocity v_{air} =330 m/s, so that fabrication of deep holes with $w << \lambda_{air}$ can be easily achieved). At higher frequencies in air, Additive Manufacturing (AM) techniques such as micro-stereolithography can be used [9,16].

If now ultrasonic signals in water are to be studied, as is the case here, then two things need to be considered – the features of the metamaterial will be smaller, and the material has to be chosen so that complications due to coupling of acoustic energy into the substrate are avoided. Consider first the required features for an ultrasonic frequency of 300 kHz in water, where v_{water} = 1480 m/s, and hence λ_{water} = 4.93 mm. It is known that the lateral size (w) of each hole needs to be $< \lambda/5$ for metamaterial behaviour [14], i.e. < 1 mm. In addition, FP transmission peaks will occur at resonances defined by the plate thickness (and hence channel length) d. Note that w is generally much smaller than d in acoustic metamaterials, and the FP structure supports multiple resonances with frequencies between f_1 and f_{max} [9], as follows:

$$f_k = k\,v/2d \text{ , with } k = 1, 2., .., k_{max} \quad (1)$$

$$f_{max} = v/w \quad (2)$$

The fundamental (the lowest frequency) FP resonance occurs at a frequency of $f_1 = v/(2d)$ (or $\lambda = 2d$), noting that the highest permitted resonance frequency (f_{max}) occurs when the wavelength is equal to the smallest hole width w (also known as the ballistic regime). Note that there is some evidence that using higher-order resonances at a fixed frequency gives better metamaterial performance in terms of evanescent wave coupling [4]. To calculate the FP resonance frequency, the effective length of the hole should be calculated, and this requires calculation of an end correction for resonances within a pipe with two open ends [17]. The end correction for a pipe (or channel) with perfectly-reflecting walls is given by [18]:

$$\Delta l = 2(0.33w), \quad (3)$$

where Δl is the distance that should be added to the length of the pipe (which then reduces the value of f_k). Note that the amount of correction decreases at higher frequencies (where λ become smaller for a fixed w [19]).

The choice of solid plate material within which the holes are to be fabricated is determined in part by the specific acoustic impedance the material (Z), which is the product of density and acoustic velocity of a given material. As an example, the typical value for Nylon is Z_{Ny} = 1.32 MPa. s/m, whereas that for air is Z_{air} = 420 Pa. s/m. This difference is required to ensure that the acoustic signal stays within the air channels, and does not couple into the solid and cause it to vibrate. In air, the large acoustic impedance mismatch makes this very easy to achieve. However, in the present case, we wish to investigate FP operation in water, for subsequent use in biomedical imaging. The value for water (Z_{water} = 1.5 MPa. s/m) is much closer to that of many solid materials such as polymers which could be used to form the metamaterial structures, so it is important to fabricate the structures using a material with a relatively high acoustic velocity and density. As an illustration, consider aluminium (Z_{al} = 17.06 MPa. s/m) and Nylon (Z_{Ny} = 1.32 MPa. s/m). Note that the value of Z_{Ny} is much closer to that of water (Z_w). As a result, the acoustic transmission coefficient (T) from water into the solid is 0.08 for aluminium and 0.53 for Nylon, calculated using the formula:

$$T = 2Z_{water}/ (Z_{solid} + Z_{water}), \quad (4)$$

where Z_{solid} is the acoustic impedance of the solid in question. Thus, acoustic energy will be much more easily transferred into a typical polymer than a metal.

Fabrication of acoustic metamaterials is one of the major challenges that limit their widespread applications [20]. Here, AM is proposed as a key enabling technology, allowing complex geometries to be realised in different length scales, which is not obtainable using conventional manufacturing methods [21,22]. Note that there have been some contributions made regarding the use of AM in the fabrication of different types of acoustic metamaterials using polymer structures (Phononic crystals [23], broadband absorbers [24] and FP structures [11,15,16,20]). However, as stated above, the acoustic impedance of polymers is not sufficiently high for operation in water to confine the acoustic signal within the subwavelength holes [16]. A recent paper [25] has demonstrated that a perforated steel plate, manufactured using conventional machining, could operate as an effective metamaterial for acoustic cloaking over the 7 – 12 kHz range. They thus showed that metallic structures are a good choice for use in water. In our case, with target frequencies of 200–800 kHz, and with the need to change hole dimensions and shapes, the fabrication method needed to change, as sub-millimeter accuracy would be needed.

Powder Bed Fusion (PBF) techniques such as direct Selective Laser Machining (SLM) are capable of fabricating reproducible metal structures with this accuracy. Processing of aluminium, titanium and nickel-based alloys in SLM is well established, and this could benefit the

widespread employment of acoustic metamaterials for enhanced imaging. In this study, SLM is used for the first time to fabricate perforated metallic plates containing arrays of through-thickness sub-mm width holes, for use at ultrasonic frequencies in water. The acoustic response of these structures was tested in through-transmission mode and conclusions are drawn on their performance by comparing experimental measurements with Finite Element simulations. SLM also allows for changes in hole geometry, such as flaring the entrance and exit, thus changing the bandwidth and frequency of operation. Sub-wavelength imaging is presented, illustrating that SLM is an ideal fabrication route for acoustic metamaterials of this type operating at ultrasonic frequencies.

2. Experimental methods

2.1. Sample design and fabrication

Initial samples of A20X aluminium were prepared using a Renishaw AM250 SLM machine. The main motivation in using the AM250 initially was its larger build platform that accommodated multiple samples in one build. A range of samples with hole dimension starting from 0.4 mm to 1.5 mm were fabricated. Samples with hole width (w) of 0.8 mm were chosen because it was the smallest hole size that could be fabricated reproducibly with minimum blockage and distortion. It was important to make the holes as small as possible, as the metamaterial function degrades as w increases. Hence, we considered the stated hole size range as the best compromise between performance and ease of fabrication. Each sample contained a 24 × 24 grid of square holes, each having a width (w) of 0.8 mm. Each hole was separated from its nearest neighbour by 0.4 mm (i.e. with a lattice constant $a = 1.2$ mm) across the overall sample dimensions of 30 mm square. Various sample thicknesses (d) were fabricated in the 5 − 9 mm range, this range being chosen to have FP resonant frequencies in a convenient frequency range for ultrasonic measurements in a water tank at frequencies of 200 − 800 kHz (where λ_{water} ranges from 18.5 − 7.4 mm).

The SLM fabrication process was started by adding the support structure to the designed CAD model (Fig. 1(a)). Note that although third-party software could be used to generate the support structure, the supports had to be aligned manually to avoid blocking the holes. Materialize Magics 2.1™ was used to slice the file and prepare the build file. A Renishaw AM250 SLM printer with a laser power of 200 W and a laser spot size of 150 μm was used in fabrication of the samples. In order to produce uniform vertical sub-millimetre channels, and to avoid having support structures within the holes, supports were used to create a 3 mm gap between the sample and the build platform, with the structures supported horizontally. This process both anchored the structure and helped with heat dissipation, preventing thermal warping and simplifying sample removal. It was also critical to avoid having support structure directly underneath the vertical channels, which might have produced blocked channels and would have therefore introduced unwanted further post-fabrication processing steps. After completing the fabrication process, the structures were cut from the build platform and the remaining support structures were ground away to leave a flat face. Fig. 2 is a photograph of a typical 30 mm square aluminium sample fabricated using SLM, with an expanded view showing some details of the nature of each hole.

Various features can be seen. First, it is evident that material adhered to the sidewalls of the holes, giving them an irregular appearance. Although these features are difficult to quantify exactly, an estimate made using a Bruker Contour GT optical profilometer. The overall surface area, measured over a number of holes, was found to be in the range 0.46 ± 0.1 mm^2 (noting that a $w = 0.8$ mm hole would have a surface area of 0.64 mm^2.) These were thus smaller than expected, and the likely effect of this will be discussed below. Note that the shortest wavelength λ_{water} of ultrasound in water encountered in this work (at the maximum frequency of 800 kHz) was ~ 2 mm. It was thus decided that the features encountered within the SLM-fabricated structures were acceptable, noting that most experimental measurements were in fact taken in the 300 − 500 kHz frequency range, where λ_{water} ranges from ~3 − 5 mm. Although work on Kelvin cell acoustic metamaterials has accurately produced strut diameters down to 0.4 mm using SLM [26], here we are dealing with holes, which are more difficult. It was also noted by Strano et al. [27] that surface roughness, caused by the staircase effect, balling and particles bound at the edges (as observed in this study) were dependent on the powder size distribution. With a vertical orientation the bound particles are the primary source of roughness. In our case, the size distribution of the aluminium powder particles was from 20 to 60 μm, leading to the observed roughness within the holes.

A second set of samples was fabricated using a Realizer SLM 50 machine with a laser spot size of 30 μm and a laser beam power of 120 W. The smaller laser spot size compared to the Renishaw AM250 above translated to smaller melt pool which potentially increased the build resolution. This was needed to demonstrate the capability of AM in changing the hole profile, with flared entrance and exit points. Such modifications can improve the performance of FP metamaterial structures and is a topic of interest in this field [15]. The titanium samples, fabricated using an average particle size of 36 μm for the build, contained a set of single holes, separated by large hole-to-hole distances (a) so that isolated FP resonances could be studied without significant acoustic interaction between each other. A photograph of the top surface of containing four such isolated holes is shown in Fig. 3, with flare radii as indicated in Table 1. The roughness of each flare profile was measured to vary in R_a value from 60 − 160 μm, depending on position across the flare, as also indicated in Table 1. It can be seen that the SLM process has been able to create these structures well, in this case in a 5 mm thick sample. Note that the roughness of the top flat surface was measured to be $R_a = 10$ μm. In relation to the surface roughness of the flare, Strano et al. [27] also demonstrated the importance of surface angle on the produced roughness, and this may be an explanation of the differences between each hole.

2.2. Ultrasonic testing

The testing of the samples at ultrasonic frequencies was performed in a custom-built testing tank filled with water at room temperature (20°C +/− 2°C). The ultrasonic source was usually a 19 mm diameter Panametrics U8517150 ultrasonic immersion transducer with a centre frequency of 500 kHz, although other sources such as piezocomposite devices were used if, for example, a lower frequency of 300 kHz was required. The samples were tested in through-transmission, with the source transducer typically placed within a cylindrical waveguide (see Fig. 4) to help ensure that the incident wave was as close to a plane wave as possible, *i.e.* had a flat wavefront. A Panametrics 5072PR ultrasonic pulser-receiver was used to excite the transmitter transducer with a high voltage step waveform. A sample holder was designed and fabricated so that the metamaterial sample could be positioned reproducibly in a plane perpendicular to the waveguide axis via a slot in the holder. The receiver was a Precision Acoustics™ 0.5 mm diameter needle hydrophone, positioned at a known distance from the metamaterial surface. The waveguide/sample holder and the ultrasonic receiver could both be positioned independently within the water tank using a dual 3-axis scanning system under PC control. The through-transmitted signals were acquired using a digital oscilloscope (Tektronix DPO7104) and transferred to a PC for post-processing. In practice, the waveguide/sample holder assembly was kept in a fixed location and the hydrophone moved to a specific location (such as over a hole). The hydrophone could also be scanned horizontally so as to sample the ultrasonic beam characteristics both with and without the metamaterial present in the holder, thus measuring its effect.

The transmission characteristics of a given sample were measured in a two-step process. First, a reference waveform was recorded at a

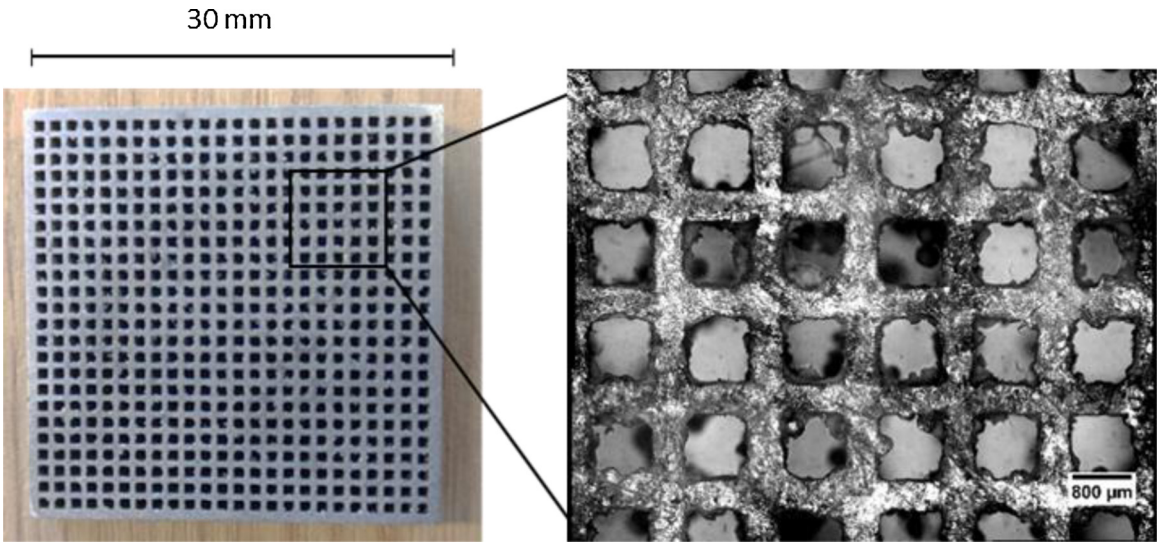

Fig. 2. Photograph of the aluminium metamaterial fabricated using SLM with d = 8 mm and w = 0.8 mm, with an expanded photomicrograph of the top surface also shown over the indicated area.

specific location without the sample being present in the sample holder between the source and receiver. The sample was then placed in the sample holder between the transducers and the signal transmitted through the structure was measured. FFTs were used to obtain the frequency spectra of these two measurements, so that dividing these two spectra allowed the effect of the metamaterial sample to be measured in the frequency domain.

3. Finite element (FE) simulations

Acoustic transmission through sub-wavelength sized square holes in SLM-fabricated samples was modelled using COMSOL Multiphysics®. An 80 µm tetrahedric mesh size was used so to have at least 10 elements to cover the channel width *w*. This was needed to confirm that the designs would produce FP resonant peaks, as required of a metamaterial, and that a metal substrate was necessary (and not a more easily-printed polymer substrate). A plane-wave ultrasonic wave of pressure amplitude 1 Pa travelling perpendicular to the sample surface was used to study the acoustic transmission of the solid sample containing holes, and a transmission coefficient extracted for each frequency.

The first task was to study the effect of acoustic impedance mismatch on the production of the FP peaks for a single 0.8-mm square hole. As stated earlier, the greater the difference in acoustic impedance *Z* between water and the solid substrate the greater the transmission of

Table 1
Details of the four holes for the sample shown in Fig. 3.

Hole number	1	2	3	4
Measured flare radius (mm)	0.15	0.28	0.74	1.6
R_a value (µm)	63	61	114	160

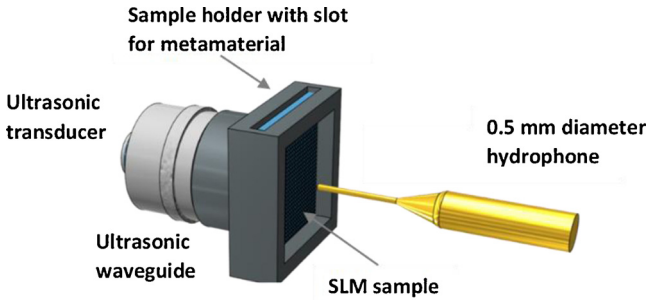

Fig. 4. Ultrasonic testing apparatus where the source transducer was placed within a cylindrical waveguide. The metamaterial sample was held in place using the sample holder shown. The receiver was a 0.5 mm diameter hydrophone, used to measure the response at the exit of a single hole.

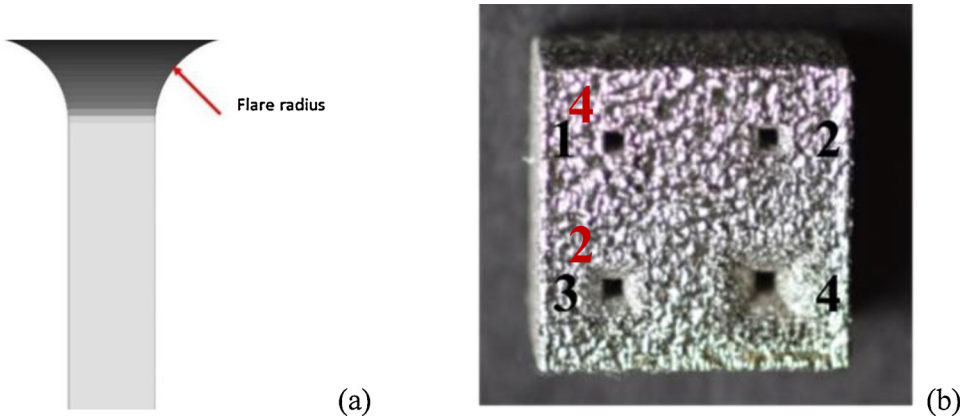

Fig. 3. (a) Illustration of a flared opening. (b)Photomicrograph of a titanium sample containing four holes (each with d = 5 mm and w = 0.8 mm), fabricated using SLM with different flare radii as detailed in Table 1. The sample had dimensions of 12 mm square by 5 mm deep.

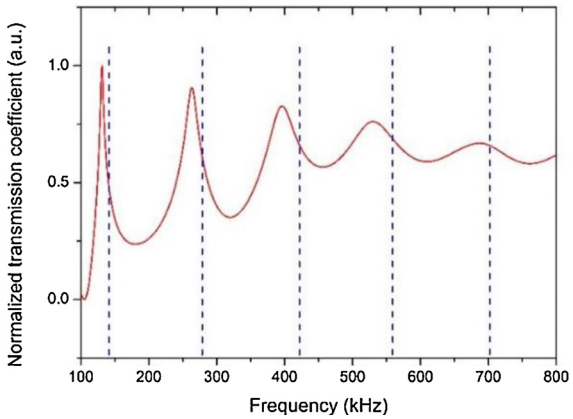

Fig. 5. Simulated response for a "hard solid" metamaterial sample in water with d = 5 mm and w = 0.8 mm. The dotted vertical lines represent the FP frequencies that are predicted by Eqs. (1) and (3).

energy into the solid, these being an unwanted phenomenon – hence the use of a metallic substrate. The first simulation was thus performed assuming a "hard solid" where no acoustic energy would flow into the solid from the water-filled hole. The result is shown in Fig. 5 for a sample thickness (d) of 5 mm. Here, the vertical dotted lines represent the positions of the FP resonance peaks expected from Eqs. (1) and (2), modified by the end correction of Eq. (3), which is a function of both the sample thickness (d) and the hole width (w). The simulation predicts the FP peaks to be a good match to the analytical expressions shown by vertical broken lines in this figure.

Simulations were also performed for aluminium and Nylon substrates, and these are plotted together with the hard solid case (where Z is assumed to be infinitely large) in Fig. 6. As noted above, Nylon is much more closely-matched acoustically to water than is aluminium (Z_{Al}), so that the acoustic transmission coefficient (T) from water into the solid is much lower for aluminium. Thus, acoustic energy will be much more easily transferred into a typical polymer than a metal. Fig. 7 shows that both aluminium and a hard solid produced clear, regularly-spaced FP peaks. Comparing the two plots, peaks for the aluminium substrate were more resonant than those of the hard solid; even though $T = 0.08$ for aluminium, this still allows some energy to leak into the metallic substrate, causing the resonance to broaden and decrease slightly in amplitude. In comparison, the "hard solid" with a perfectly-reflecting boundary would have $T = 0$, and all energy would be confined within the water column. FP resonant peaks were also shifted to lower values in the simulation than for the hard solid case. In contrast, the expected FP peaks are completely absent in the Nylon structure,

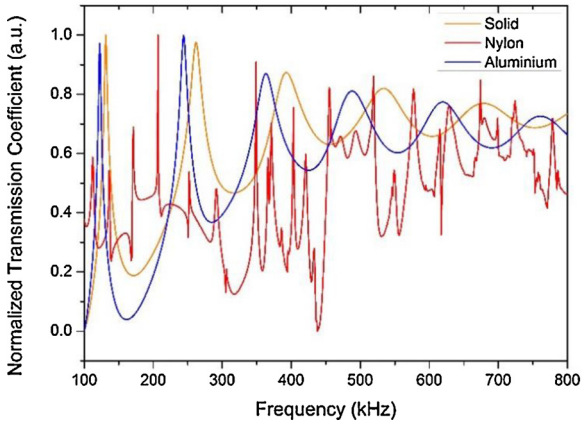

Fig. 6. Simulation results for acoustic transmission of a single 0.8-mm square hole in a d = 5 mm sample.

being replaced by an irregular distribution of resonant peaks. This is thought to be due to a large amount of acoustic cross-coupling into the solid, so that the solid substrate and water-filled columns interact in a complicated fashion.

It is known that variations in hole size and shape can affect the operation of FP-type acoustic metamaterials [13]. It has been shown above that build geometries could vary from the CAD design, and hence it was important to study the likely effect of this. By carefully studying the fabricated samples, it was clear that the holes were slightly smaller than the designed size and that they had rounded corners. Accordingly, simulations were performed to study the likely effect of 1) decreasing the symmetry in the holes, 2) reducing the dimension of the holes to represent the experimental samples, and 3) the difference between holes that were perfectly square and those with rounded corners. This used PZFlex 2018™ (OnScale Inc, USA) FE software after importing the designed CAD model from Solidworks™, which was found to be more suitable for these more complex geometries. Again, a plane-wave ultrasonic wave of pressure amplitude 1 Pa travelling perpendicular to the sample surface was used. PZFlex was implemented using a simple cubic element mesh type, with a mesh size 37 μm along all three dimenions, which is much smaller than the smallest wavelengths of interest - 50 elements per wavelenth at the highest frequency of interest (800 kHz).

The first additional simulation looked at rounding the corners of the square hole. Fig. 7(a) shows the transmission coefficient of a $w = 0.8$ mm square hole in a 5 mm thick aluminium sample compared to a similar hole with rounded corners. The rounding radius of 0.1 mm was chosen for this simulation. The transmission coefficient plot is almost identical in each case, indicating that rounded corners with this extent of feature do not affect the position and amplitude of the FP peaks. As noted in Fig. 2, the dimensions of each hole fabricated by SLM differed across the sample. It was thus interesting to see the effect of the size of the hole (w). The simulated transmission characteristics of rectangular holes with a range of dimensions are compared in Fig. 7(b). By reducing the hole width w from 0.8 mm to 0.7 mm and 0.6 mm, the resonance peaks shift from 320 kHz to 324 kHz and 330 kHz respectively which is in good agreement with the findings in the literature [10]. From the simulation it is clear that in the rectangular holes, the position of the FP resonance peak is dependent on the dimension of the smaller side of the hole. The end correction, which is dependent on the hole width w (see Eq. (3)), could be one of the main contributing factors to these small shifts.

Another area of interest is changing the shape of the holes. It is known that gradually changing the width of a hole with flared entrances and exits can help the acoustic impedance within the hole to match that in the surrounding air (noting that the restriction on airflow within the hole increases its acoustic impedance Z, which is actually the reason why FP resonances occur). Doing this is likely to decrease the Q of the resonance, and hence the bandwidth of operation, but to increase transmission amplitudes due to the greater surface area of the opening. This is of interest to ultrasonic imaging applications as it allows techniques for signal to noise enhancements (such as pulse compression) to be used, and also potentially improves image resolution. SLM is an ideal technology for the fabrication of such structures, giving flexibility over changes in hole dimensions throughout the build. For this reason, simulations were performed to study this effect. The results shown in Fig. 8 are for four cases with fixed hole dimension and thickness ($w = 0.8$ mm, and $d = 5$ mm) but with flares of 0, 0.4 mm, 0.8 mm and 1.6 mm radius. Titanium with specific acoustic impedance of $Z_{Ti} = 27.33$ MPa. s/m was assigned to the simulated structures. These predictions indicate that the effect of increasing the flare radius is to increase the amplitude of the FP resonance and shift the centre frequency to a higher value. The increase in the FP resonance amplitude means more energy is being coupled into the hole by a flared aperture. The shift in the centre frequency of the FP peak is due to change in the effective length or dimension of the hole over which the FP resonance

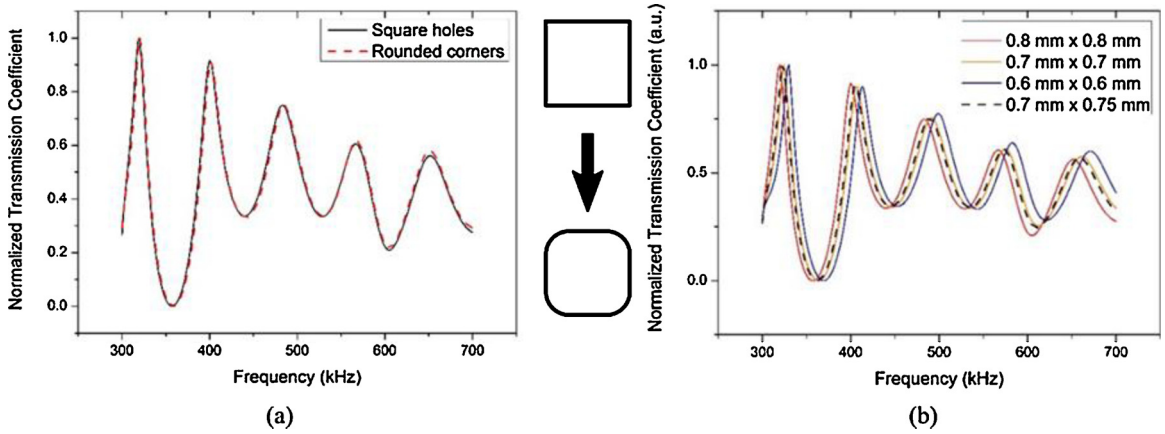

Fig. 7. (a) Normalized transmission coefficient for an aluminium sample with either a 0.8 mm square hole or one with rounded corners with a radius of 0.1 mm. Little difference in the predicted response is seen. (b) As in (a), but for a single rectangular hole with different dimensions. Decreasing the dimensions of the hole in either direction causes the FP resonance peaks to shift to higher frequencies.

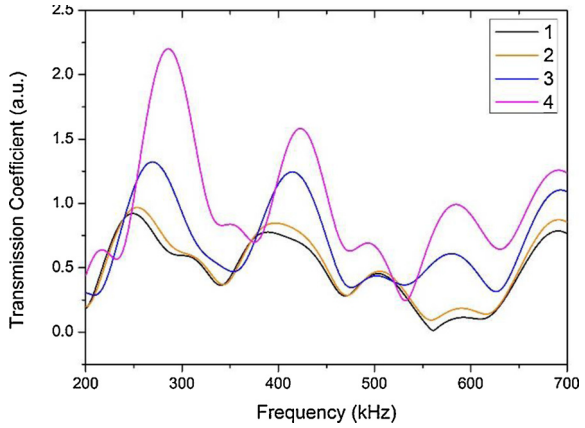

Fig. 8. FE simulations for single holes in a titanium sample with d = 5 mm. The numbered holes have different flare radii compared to a straight hole (see Table 1).

would be established.

4. Results of measurements in water

The 0.5 mm diameter needle hydrophone was used to observe the ultrasonic signal at one of the holes in an aluminium metamaterial sample with $d = 8.5$ mm and $w = 0.8$ mm. This was to confirm that FP resonances were present. An ultrasonic waveform was thus recorded with the hydrophone tip positioned at the centre of one of the holes, and at a distance of 1 mm from the sample surface. A typical time trace from an 8.5 mm thick sample is shown in Fig. 9(a). The corresponding frequency spectrum of this signal (corrected for the baseline spectrum established with the hydrophone in the water) is shown in Fig. 9(b). Based on Eqn. (1), and considering the effect of end correction, the fundamental FP resonance peak is expected to occur at a frequency (f_1) of 82.9 kHz, which is outside the −6 dB bandwidth of the transmitter. However, the 4th, 5th, 6th and 7th harmonics at frequencies $f_4 - f_7$ can be seen in Fig. 9(b). Although theoretically the transmission coefficient of structures at frequencies close to their FP resonance frequency is expected to approach unity, experimentally the signal amplitude decreases for higher harmonics (at frequencies f_4, f_5 etc. for successive harmonics) as has been observed in other studies [9]. Table 1 compares the measured FP resonant frequencies to those calculated. The good agreement indicated that the FP resonances in the metamaterial structure are present at the expected ultrasonic frequencies. Note that additional maxima and minima are present in the spectrum. This could be due to complications arising from the interaction between adjacent holes, as the hydrophone has a relatively wide angle of sensitivity at these frequencies, and could detect emission from more than one hole, complicating the received signal.

Note that the higher harmonics are not as strong in the experimental measurements as in the FE predictions in Fig. 5. This is thought to be due to scattering effects within the hole. Higher harmonics, at higher frequencies, have shorter wavelengths in water, and these are quoted for each of the harmonics $f_4 - f_7$ in Table 1 (assuming a velocity in water of 1480 ms^{-1}). Hence, ultrasonic propagation within each hole is more likely to be disrupted by the surface roughness on the inner wall at higher resonant frequencies, due to scattering effects. Energy will be lost, reducing the effectiveness in establishing a FP resonance. Thus, it is important to choose the correct operating frequency for FP effects to occur, and the upper limit will be dictated by the build resolution within the holes.

Several extra peaks are observable in Fig. 9(b) which are not primary FP resonances. The main reason is that the output is the result of interaction between the array of holes in the metamaterial. The holes couple together via evanescent waves to produce metamaterial effects, but this only occurs within distances $< \lambda_{water}$. However, cross coupling between the channels via conventional ultrasonic propagation along the surface of the sample is possible, and this could produce extra peaks in the normalised transmission coefficient [2]. It is interesting to note that there is very good agreement between the theoretical and experimental values for the resonant frequencies in Table 1, showing that the simple formula of Eq. (1) is a good predictor of the resonant frequency in samples containing either multiple or single holes (Table 2).

Because of the difficulty in eliminating interactions between closely spaced holes in the metamaterial sample, further studies were performed with samples which contained only a single hole. This allowed both single square holes and the effect of flaring of the aperture to be measured experimentally and compared to the FE simulations shown earlier in Fig. 8. Samples were available with various radii of curvature of the flare (photographs of the SLM-fabricated samples were shown earlier in Fig. 3). Experimental results are presented in Fig. 10 to compare directly to the FE simulations, where it can be seen that simulation and experiment show the same trends as a function of flare radius for holes 1 − 3. This indicates that the effect of increasing the flare radius is to increase the amplitude of the FP resonance (due to greater energy transfer into and out of the hole) and shift the centre frequency to a higher value (a flared aperture would also effectively shorten the length of the hole over which the FP resonance would be established). Note, however, that experimentally the main resonant frequency reduced less markedly than in simulations as the flare radius increased. This could be due to the stepped features already noted in

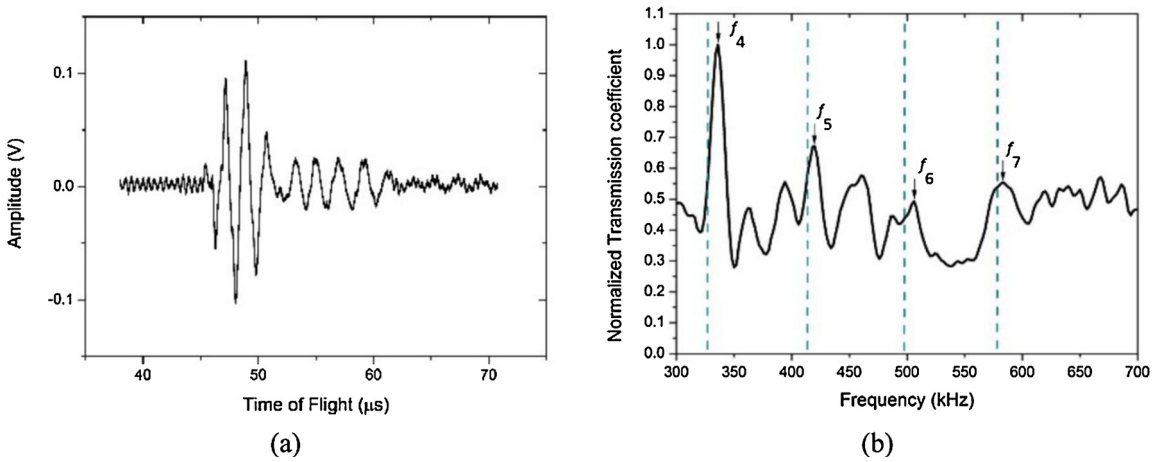

Fig. 9. (a) Recorded ultrasonic time waveform and (b) corresponding frequency spectrum of ultrasonic signals received by a 0.5 mm needle hydrophone centred on one of the holes in a multi-hole sample. Vertical dashed lines show the theoretical locations of the FP resonance peaks (with the end correction applied) from Eqs. (1) and (3). The experimental FP peaks are marked with arrows and the harmonic number.

Table 2
Calculated and measured values of FP resonant frequencies from Fig. 10, together with the calculated wavelength in water in each case for the experimentally-measured FP peak.

FP resonance harmonic	f_4	f_5	f_6	f_7
Theoretical value (kHz)	332	415	497	580
Experimental measurement (kHz)	336	418	504	584
Ultrasonic wavelength in water at the frequency measured experimentally (mm)	4.41	3.54	2.94	2.53

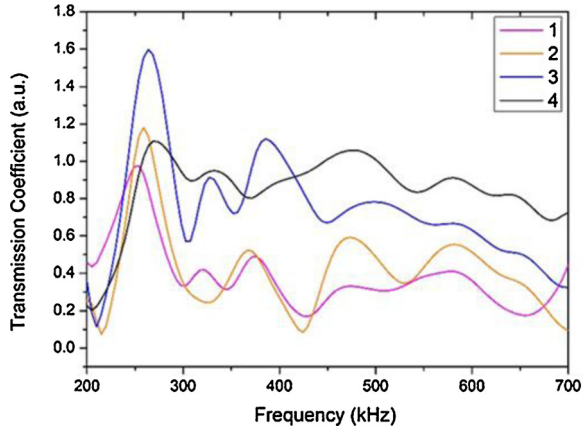

Fig. 10. Experimental results for widely-spaced single holes in a titanium sample (with d = 5 mm, shown earlier in Fig. 3 and with the features given in Table 1). The numbers refer to the holes as labelled in Fig. 3.

the fabricated sample. The main difference between the simulation and experimental results is in hole 4, where experimentally the expected strong resonance has not been established. This indicates that FP resonances could be difficult to establish practically at large radii of curvature. Here, the impedance mismatch between water in the hole and in free water (which allows FP resonances to be established) is lower, making any small disturbances (such as exact geometry and surface roughness) in a practical build more prominent. Note that these larger radii would also cause the lattice parameter (a) to increase due to the resultant wider spacing between holes; this would affect image resolution in a practical measurement, and hence smaller radii would be preferred in any case.

A final experiment was performed to demonstrate the imaging resolution potential of the SLM-fabricated metamaterial. To show this, the frequency of operation was chosen to be centred at 300 kHz (a frequency close to the expected FP resonance peak shown earlier in Fig. 6 for an aluminium metamaterial sample with $d = 8$ mm and $w = 0.8$ mm in water). Imaging resolution was measured by inserting a 0.7 mm ($\sim \lambda_{water}/7$ at 300 kHz) wide slit aperture of 19 mm length, machined within an additively-manufactured 4.3 mm thick PLA plate, placed between the ultrasonic transmitter and the metamaterial, as shown in Fig. 11. The slit was positioned close (< 1 mm) to the metamaterial surface. While fabricated from polymer, where some transmission was possible through the solid, The hydrophone was then scanned horizontally across the far side of the metamaterial, and at a distance of 1 mm from it (i.e. at a total distance of 9 mm from the slit aperture). The aim of this experiment was to demonstrate that the ultrasonic signal has been collected by the metamaterial, and transferred with a sub-wavelength resolution to the far side, using water as the medium. This occurs primarily because of coupling from so-called evanescent waves from each of the output holes in the metamaterial. At this frequency, the wavelength of the ultrasonic signal in water was $\lambda_{water} = 4.9$ mm, so that $\lambda_{water}/w = 6.16$. The metamaterial thus has sub-wavelength values for the hole width (w) and unit cell size (a) of 1.2 mm used. This experiment was thus a test of whether the features could be detected by the scanned hydrophone, even though the slit was less than a wavelength (λ_w) wide. Note that at a distance of 9 mm from the slit aperture, the slit would not normally be resolvable without the metamaterial in place. The slit was placed at a distance of ~0.5 mm ($\sim \lambda_w/10$) from the metamaterial – it has to be close as the evanescent waves needed for

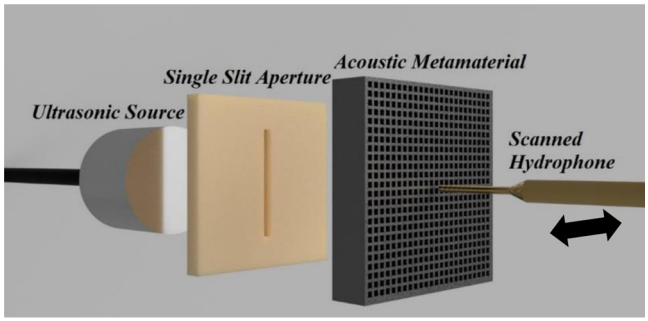

Fig. 11. Schematic diagram of the image resolution experiment at 300 kHz. This used an aperture test plate that was placed between the ultrasonic source and the metamaterial, next to the latter's surface. The miniature hydrophone receiver was then scanned in a horizontal line parallel to the output surface of the metamaterial. The ultrasonic source, slit aperture and metamaterial were held stationary during this measurement.

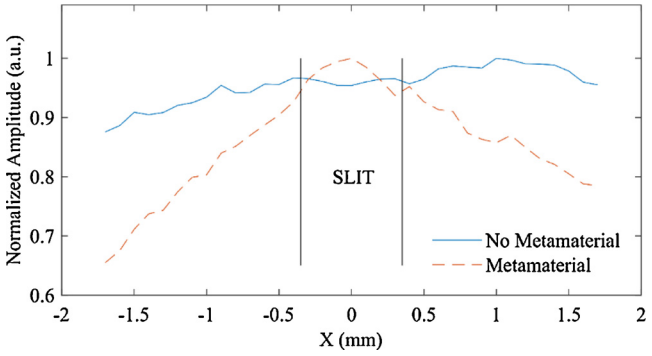

Fig. 12. Ultrasonic data taken by scanning the hydrophone across the 0.7 mm wide slit shown in Fig. 11 at a horizontal distance of 9 mm from the slit. The size and location of the slit is shown by the vertical lines.

metamaterial operation act over short distances ($< \lambda_w$). Note that there was also likely to be ultrasonic transmission through the material of the slit aperture component, but sufficient contrast would have existed to test the imaging performance in the presence of the sub-wavelength aperture.

The measurement was thus performed for the two cases, namely with and without the metamaterial in place, and the resultant normalised plots are shown together in Fig. 12(a). Note that in practice the received signal was of higher amplitude with the metamaterial absent, as would be expected due to losses at the input and output surfaces of the metamaterial. The plot with the metamaterial absent also exhibited a maximum value outside the slit region (identified by the vertical lines). This is a result of the amplitude variations across the transducer beam profile and subsequent diffraction by the slit. It can be observed that insertion of the metamaterial concentrated the energy into a smaller lateral region. Dividing these two data sets allowed the true effect of the metamaterial to be observed, as shown in Fig. 12(b). It can be seen that the slit was detected very well, even though it is sub-wavelength in width. The metamaterial uses evanescent waves to couple the ultrasonic output energy from multiple holes together, each having a Fabry-Perot resonance, to obtain these effects. The slit, being a single aperture, cannot function as a metamaterial as this coupling does not exist, but acts as a secondary acoustic source to demonstrate the detection of a sub-wavelength aperture.

It should be noted that the lateral width of the slit aperture was not detected accurately. The resolution of such a measurement depends on both the hole width (w) and the unit cell size (a) in a complicated way that we are currently investigating, and to improve this would require a smaller values of both w and a. However, the above represents the first time that such a result has been reported at these ultrasonic frequencies in water, and demonstrates how PBF fabrication techniques can be used to create metallic metamaterial structures of interest to the ultrasonic imaging community.

It is thus demonstrated that the interaction between FP resonances of the metamaterial and the evanescent waves allow us to detect features up to $\lambda_w/7$ in water and that this has been made possible by the use of SLM fabrication.

5. Conclusions

This paper has demonstrated for the first time that metallic ultrasonic metamaterials can be fabricated to operate in water at the 200–800 kHz frequency range, important for many applications such as non-destructive evaluation and medical imaging. It was demonstrated that PBF processes such as SLM processes produced metamaterials that supported Fabry–Perot (FP) resonances. The acoustic properties of fabricated structures were measured at ultrasonic frequencies, where higher-order FP resonance peaks were observed using a needle hydrophone. The need for a metallic substrate to ensure a reasonable acoustic impedance mismatch with water was demonstrated in the numerical simulations. It is also proven that flaring of the apertures at each end could be fabricated, and that this resulted in a change in the frequency response of the structure. The findings also suggest that the presence of high surface roughness did not unduly affect the generation of FP resonances within each hole of the metamaterial, although it might have been a limitation in certain builds with large flare radii. A measurement in the presence of a slit aperture demonstrated that a slit with sub-wavelength width was detected successfully in the presence of the metamaterial structure. Note that the hole dimensions used within these metamaterials, in terms of depth and width, would both have an effect on the amplitude and frequency response of the resonances within each hole. We aim to study this in future work.

CRediT authorship contribution statement

Meisam Askari: Methodology, Investigation, Writing - original draft, Software. **David A. Hutchins:** Supervision, Conceptualization, Methodology, Writing - original draft, Project administration. **Richard L. Watson:** Methodology, Investigation, Writing - review & editing. **Lorenzo Astolfi:** Methodology, Investigation, Writing - review & editing, Software. **Luzhen Nie:** Methodology, Investigation, Writing - review & editing, Software. **Steven Freear:** Supervision, Conceptualization. **Peter J. Thomas:** Supervision, Methodology, Writing - review & editing. **Stefano Laureti:** Methodology, Software. **Marco Ricci:** Methodology. **Matt Clark:** Supervision. **Adam T. Clare:** Supervision, Methodology, Project administration.

Declaration of Competing Interest

The authors declare that they have no known competing financial interests or personal relationships that could have appeared to influence the work reported in this paper.

Acknowledgements

Funding for this work was provided through the Engineering and Physical Sciences Research Council (EPSRC), Grant numbers EP/N034163/1, EP/N034201/1 and EP/N034813/1. The authors would like to acknowledge the help and support of Mr Mark Hardy and Dr Ian Maskery.

Appendix A. Supplementary data

Supplementary material related to this article can be found, in the online version, at doi:https://doi.org/10.1016/j.addma.2020.101309.

References

[1] S. Guenneau, R.V. Craster, Acoust. Metamaterials SE - 1, Springer, 2013, pp. 1–42.
[2] H. Estrada, P. Candelas, A. Uris, F. Belmar, F.J. García De Abajo, F. Meseguer, Appl. Phys. Lett. 95 (2006–2009) (2009).
[3] B. Hou, J. Mei, M. Ke, W. Wen, Z. Liu, J. Shi, P. Sheng, Phys. Rev. B - Condens. Matter Mater. Phys. 76 (2007).
[4] J. Zhu, J. Christensen, J. Jung, L. Martin-Moreno, X. Yin, L. Fok, X. Zhang, F.J. Garcia-Vidal, Nat. Phys. 7 (2011) 52–55.
[5] S.A. Cummer, J. Christensen, A. Alù, Nat. Rev. Mater. 1 (2016) 16001.
[6] Y. Cheng, C. Zhou, Q. Wei, D. Wu, X. Liu, Appl. Phys. Lett. 103 (2013).
[7] N. Engheta, R.W. Ziolkowski, Metamaterials (2006).
[8] J. Christensen, L. Martin-Moreno, F.J. Garcia-Vidal, Phys. Rev. Lett. 101 (2008).
[9] S. Laureti, L.A.J. Davis, M. Ricci, D.A. Hutchins, IEEE Int. Ultrason. Symp. IUS (2014) 1344–1347.
[10] S. Laureti, D.A. Hutchins, L.A.J. Davis, S.J. Leigh, M. Ricci, AIP Adv. 6 (2016) 121701.
[11] H. Estrada, F.J.G. De Abajo, P. Candelas, A. Uris, F. Belmar, F. Meseguer, Acoust. Metamater. (2013), pp. 83–113.
[12] M.H. Lu, X.K. Liu, L. Feng, J. Li, C.P. Huang, Y.F. Chen, Y.Y. Zhu, S.N. Zhu, N. Ben Ming, Phys. Rev. Lett. 99 (2007).
[13] H. Estrada, P. Candelas, A. Uris, F. Belmar, F.J. García De Abajo, F. Meseguer, Phys.

Rev. Lett. 101 (2008) 2–5.
[14] H. Estrada, Ultrasonic Transmission Through Periodically Perforated Plates, Universidad Politécnica de Valencia, 2011.
[15] K.K. Amireddy, K. Balasubramaniam, P. Rajagopal, Appl. Phys. Lett. 108 (2016).
[16] S. Laureti, Acoustic Metamaterials for Medical Ultrasound and Non-Destructive Evaluation, Warwick University, 2016.
[17] Y. Tang, S. Ren, H. Meng, F. Xin, L. Huang, T. Chen, C. Zhang, T.J. Lu, Sci. Rep. 7 (2017) 1–11.
[18] T. Boelkes, I. Hoffmann, ISB J. Phys. (2011) 1–3.
[19] J. Nat. Sci. Res. 3 (2013) 21–24.
[20] F. Lucklum, M. Vellekoop, Crystals 7 (2017) 348.
[21] Y. Liao, Y. Chen, G. Huang, X. Zhou, J. Appl. Phys. 123 (2018) 90901–230901.
[22] C.R. Garcia, J. Correa, D. Espalin, J.H. Barton, R.C. Rumpf, R. Wicker, V. Gonzalez, Prog. Electromagn. Res. Lett. 34 (2012) 75–82.
[23] S. Laureti, O. Akanji, L.A.J. Davis, S.J. Leigh, D.A. Hutchins, M. Ricci, Proc. 2015 IEEE Int. Ultrason. Symp. (IEEE, Taiwan) 1 (2015) 3–6.
[24] M. Yang, S. Chen, C. Fu, P. Sheng, Mater. Horizons 4 (2017) 673–680.
[25] P.A. Kerrian, A.D. Hanford, D.E. Capone, B.S. Beck, J. Acoust. Soc. Am. 146 (2019) 2303.
[26] H.J. Rice, J. Kennedy, P. Göransson, L. Dowling, D. Trimble, J. Sound Vibr. 472 (2020) 115167.
[27] G. Strano, L. Hao, R.M. Everson, K.E. Evans, J. Mater. Process. Technol. 213 (2013) 589–597.